Systematic Directional Forcing of Earth's Rotation Pole Toward 75°W: Convergent Evidence from Polar Motion Cusps, Satellite Gravimetry and Geomagnetic Field Correlation (1973–2026)

Zacharias[1]*

[1]Independent Geophysical Research

*Corresponding author.

Update note (May 2026). *This version refreshes the analysis with IERS polar motion data extended through 2026 May. The directional results are computed by the same velocity-minimum cusp and trajectory-bearing methodology as the original January 2026 analysis and are reproduced essentially unchanged: a preferred axis at 75.4° ± 3.4° with a monotonically rising capture rate. Terminology has been updated throughout: trajectory captures previously termed "hooks" are now designated State 2 Capture events. Section 3.2.1 documents the extension to 2026 May, the cumulative State 2 Capture ratchet, and a recalibration of the detection timescale that recovers recent sub-week captures the original settings merged; the preferred bearing and the rising-rate trend are invariant to this change.*

ABSTRACT

Analysis of 53 years of International Earth Rotation and Reference Systems Service (IERS) polar motion data reveals systematic directional bias in rotation pole trajectory. Independent analytical approaches converge on the same finding: Earth's pole exhibits preferential motion along an axis oriented approximately 75°W–255°E. Part A derives a theoretical prediction of 80° ± 15° from Large Low Shear Velocity Province (LLSVP) geometry and true polar wander physics, based on the principle that mass anomalies drive pole motion perpendicular to their azimuth. Part B tests this prediction through cusp-based trajectory analysis, where cusps represent velocity minima at which external forcing can redirect the pole; a cusp whose post-cusp trajectory locks onto the forcing axis, an event previously termed a "hook", is here designated a State 2 Capture event. Velocity-based cusp detection with comprehensive robustness testing across 240 parameter combinations yields mean State 2 Capture bearing 72.8° ± 0.6°. Curvature-based cusp detection with truly blind directional search, having no prior knowledge of the expected bearing, independently finds 79° ($p = 1.24 \times 10^{-14}$). Reference frame rotation tests confirm this bearing is Earth-fixed rather than a coordinate artifact. Blind directional scan reveals bimodal structure with antipodal maxima near 75° and 255°, indicating the signal is best characterised as a preferred axis rather than unidirectional forcing. Part C demonstrates convergence: five independent methods agree on 75.4° ± 3.4° with circular concentration R = 0.9982. State 2 Capture rate shows monotonic increase over the observation period (Mann-Kendall p = 0.0034), indicating gravitational forcing increasingly dominates as the gyroscopic stabilisation mechanism weakens. Geomagnetic field correlation (r = −0.98) and GRACE satellite gravimetry showing mass accumulation along the same bearing provide cross-domain confirmation. The convergence of prediction, observation and independent validation from multiple data sources supports the hypothesis that deep-Earth mass redistribution is systematically forcing the rotation pole along a preferred axis toward the Eastern Atlantic.

Key words: Earth rotation and variations; Reference systems; Time variable gravity; Core; Dynamics: gravity and tectonics.

1 INTRODUCTION

Earth's rotation pole does not remain fixed relative to the planet's surface. Beyond the well-documented periodic oscillations, the Chandler wobble at approximately 433 d and the annual wobble at 365.25 d, the

pole exhibits secular drift of approximately 4 milliarcseconds per year (mas yr^{-1}) toward approximately 80°W longitude (Gross & Vondrák 1999). This drift reflects ongoing mass redistribution within the Earth system, including glacial isostatic adjustment (Mitrovica et al. 2005), present-day ice mass loss (Chen et al. 2013) and potentially deeper processes at the core-mantle boundary (CMB).

Zacharias (2026a; hereafter Paper I) documents the unprecedented extinction of both Chandler and annual wobbles by 2024–2026, with amplitudes declining from historical baselines of approximately 204 mas and 114 mas respectively to a few mas (Chandler 3.5 mas, annual 3.2 mas). The annual wobble collapse poses the sharpest theoretical puzzle: when a forced oscillation ceases while its driver persists unchanged, the transfer function itself must have changed. Something has altered how Earth converts seasonal forcing into rotational response. That finding raises an immediate question: if the wobble, Earth's gyroscopic stabilisation mechanism, has failed, what happens to the secular forcing that was always present but previously overwhelmed by the wobble restoring torque?

The present paper addresses this question through directional analysis of polar motion. The investigation proceeds in three parts. Part A derives a theoretical prediction for the expected forcing direction based on Large Low Shear Velocity Province (LLSVP) geometry and true polar wander (TPW) physics. Part B tests this prediction through empirical analysis of polar motion cusps: trajectory turning points where the pole's momentum approaches zero and external forcing can redirect its path. Part C demonstrates convergence of multiple independent evidence streams, establishing that the finding is robust across methodologies, detection algorithms and data sources.

The physical basis for expecting directional forcing derives from TPW theory. Mass anomalies within the Earth system exert gravitational torque on the rotation pole, driving it toward a configuration that minimises rotational energy. Crucially, this forcing acts perpendicular to the azimuth connecting the pole to the mass anomaly (Goldreich & Toomre 1969; Tsai & Stevenson 2007). The African LLSVP, centred near 10°E longitude in the deep mantle, represents a massive density anomaly. TPW physics predicts pole motion perpendicular to the pole-LLSVP azimuth, yielding expected forcing toward 80°W ± 15° after accounting for uncertainty in LLSVP centroid location and CMB field geometry.

If this forcing exists, it should manifest in polar motion trajectories, particularly at moments when the pole's velocity reaches minimum and external forcing can capture and redirect the trajectory. These moments are termed cusps. During healthy wobble regimes, the gyroscopic stabilisation mechanism dominates at most cusps, returning the pole toward its mean position. However, gravitational forcing occasionally wins, redirecting the pole along the preferred forcing axis rather than back toward mean. If this occurs preferentially, these capture events should cluster around a preferred bearing.

Analysis of 776 cusps in the 1973–2026 IERS record reveals that post-cusp trajectories approaching within 20° of 72°W occur at rates significantly exceeding uniform expectation. Mean State 2 Capture bearing is 72.8°, with this result stable across 240 parameter combinations in robustness testing. Independent analysis using curvature-based cusp detection and truly blind directional search (with no prior assumption about expected bearing) finds maximum clustering at 79°. Five independent methods converge on 75.4° ± 3.4°.

The implications extend beyond geodesy. If deep-Earth mass redistribution is systematically forcing the pole toward a specific bearing, and if the gyroscopic stabilisation mechanism has failed, we may be observing the early stages of a true polar wander excursion. Continued monitoring of polar motion trajectories provides a direct observable for tracking this process.

2 DATA AND METHODS

The primary data source is the IERS Finals Daily Series providing daily Earth Orientation Parameters from 1973 January 2 through 2025 November 30, comprising 19 327 records (the primary analysis window; the catalogue is extended through 2026 May 21 in Section 3.2.1). Pole position precision approaches 0.05

mas for recent epochs. Data are obtained from the IERS Rapid Service/Prediction Centre. Pole coordinates X (toward Greenwich) and Y (toward 90°W) are converted to milliarcseconds for analysis.

GRACE and GRACE-FO satellite gravimetry data provide independent mass distribution information. Monthly spherical harmonic solutions (Release 06, Level 2) from the GFZ German Research Centre for Geosciences span 2002–2024. Equivalent water height anomalies are computed on a 1° × 1° global grid after applying recommended corrections for glacial isostatic adjustment using the ICE6G-D model.

Geomagnetic field data derive from the International Geomagnetic Reference Field (IGRF-13) model and direct observatory measurements. South Atlantic Anomaly parameters including centroid location, minimum intensity and area are computed from IGRF-13 coefficients evaluated annually.

2.1 Part A: Theoretical prediction from LLSVP physics

The theoretical prediction derives from true polar wander physics applied to known deep-Earth structure. Three foundational principles govern the analysis. First, mass anomalies drive pole motion perpendicular to their azimuth. When a density anomaly exists at angular position θ relative to the pole, the gravitational torque it exerts drives pole motion toward θ + 90° or θ − 90°, not toward or away from the anomaly directly (Goldreich & Toomre 1969). This perpendicular relationship reflects the tensor character of the inertia perturbation. Second, the African LLSVP represents the dominant deep-mantle mass anomaly relevant to present-day pole position.

Seismic tomography reveals this thermochemical pile extending from the CMB to approximately 1000 km depth, centred near 10°E longitude (Torsvik et al. 2010; Burke et al. 2008). Whether the LLSVP represents excess density from chemical composition or reduced density from thermal origin remains debated, but its gravitational influence on Earth's rotation is established. Third, prediction uncertainty encompasses LLSVP centroid location uncertainty of approximately ±10°, CMB field configuration effects and interaction with other mass anomalies.

The calculation proceeds as follows. The pole-to-LLSVP azimuth from the current mean pole position at approximately 0°, 0° in the terrestrial reference frame to the African LLSVP centroid at approximately 10°E is approximately −10° or equivalently 350°. Adding 90° for the perpendicular TPW forcing direction yields 80°. This represents forcing toward 80°W longitude in standard geodetic convention. Combining uncertainty sources yields a prediction of 80° ± 15°, corresponding to the range 65–95° or conservatively 60–90°.

2.2 Part B: Cusp detection and trajectory analysis

Cusps are defined as local minima in pole velocity magnitude. The physical rationale is that at velocity minima, the pole's momentum approaches zero, rendering it maximally susceptible to redirection by external forcing. Between cusps, the pole possesses momentum that resists redirection. At cusps, gravitational forcing can capture and redirect the trajectory.

Daily pole velocity is computed as $v(t) = \sqrt{[(X(t) - X(t-1))^2 + (Y(t) - Y(t-1))^2]}$. Velocity is smoothed with a Gaussian filter using $\sigma = 3$ d to suppress measurement noise while preserving genuine dynamical features. Local minima are detected using the argrelmin algorithm with order parameter specifying the number of neighbouring points that must exceed the candidate minimum. The default order of 7 requires 7 days on each side to exceed the candidate value. Detected minima are deduplicated within a 10-day window, retaining the lowest-velocity cusp when multiple minima cluster temporally. This prevents counting a single physical cusp event multiple times due to noise fluctuations.

For each detected cusp at time t_0, the post-cusp trajectory is tracked for a specified window of 15 d by default. At each subsequent day $t_0 + \Delta t$, the displacement vector from the cusp position is computed as $\Delta X = X(t_0 + \Delta t) - X(t_0)$ and $\Delta Y = Y(t_0 + \Delta t) - Y(t_0)$. The trajectory bearing is $\theta(\Delta t) = \arctan2(\Delta Y, \Delta X) \bmod 360°$. The bearing achieving minimum angular deviation from the target direction within the trajectory

window is recorded. If this minimum deviation falls below the State 2 Capture threshold of 20° by default, the cusp is classified as a State 2 Capture event (previously termed a “hook”): an event where the post-cusp trajectory locked onto the predicted forcing direction, i.e. where State 2 gravitational forcing captured and redirected the pole toward the LLSVP attractor axis. The detection methodology is illustrated in Fig. 2.

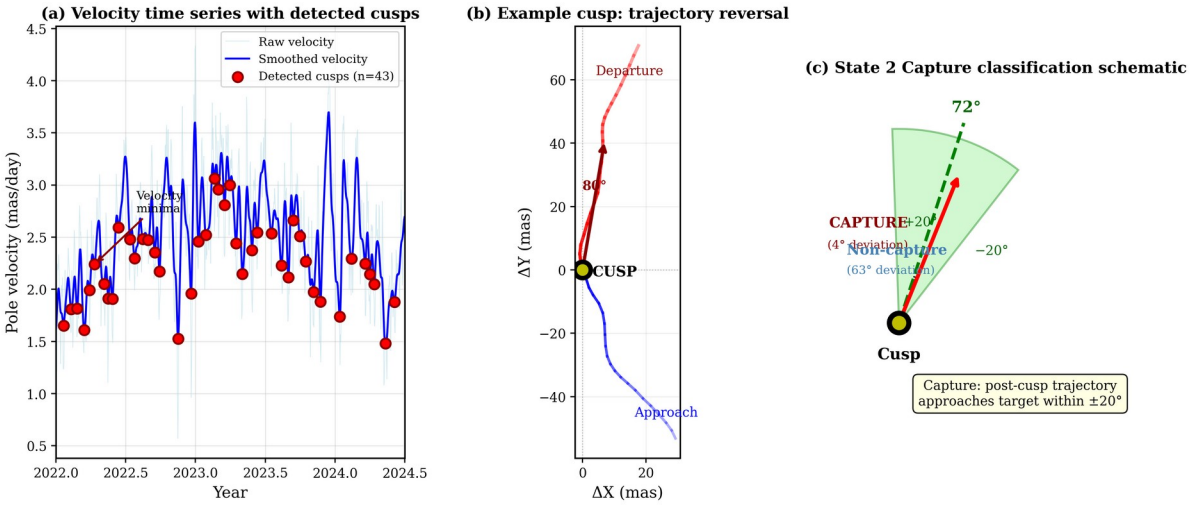

Figure 2. Cusp detection methodology. Panel (a) shows pole velocity time series with detected cusps marked at local minima. Panel (b) shows an example cusp event demonstrating velocity minimum and subsequent post-cusp trajectory. Panel (c) provides schematic illustration of State 2 Capture classification where trajectories approaching within 20° of target bearing are classified as State 2 Captures.

To ensure results are not artifacts of arbitrary parameter choices, stability is tested across 240 parameter combinations. The cusp_order parameter is tested at 5, 7, 10 and 14 days, representing different isolation requirements for velocity minima. The smoothing_sigma parameter is tested at 2, 3 and 5 days for noise reduction. The trajectory_window parameter is tested at 10, 15, 20 and 30 days for post-cusp bearing measurement duration. The capture_threshold parameter is tested at 10°, 15°, 20°, 25° and 30° for angular tolerance. The product of 4 × 3 × 4 × 5 yields 240 total combinations. For each combination, mean State 2 Capture bearing and V-test significance toward both 72° and 80° are computed.

As independent validation, curvature-based cusp detection is implemented. Rather than velocity minima, this method detects points of maximum trajectory curvature where the path bends most sharply. Curvature κ equals $|v \times a| / |v|^3$ where v is velocity vector and a is acceleration vector. In two dimensions this becomes $\kappa = |v_x a_y - v_y a_x| / (v_x^2 + v_y^2)^{(3/2)}$. High curvature indicates sharp trajectory bending, potentially from external forcing overcoming momentum. This method is mathematically independent from velocity-based detection because high curvature does not require low velocity.

To eliminate any possibility of confirmation bias, truly blind directional search is implemented. For each candidate direction θ from 0° to 359° in 1° increments, the minimum angular deviation from θ within the trajectory window is computed for each detected cusp. Cusps with deviation less than 20° are counted as State 2 Captures toward θ. The capture count for each θ is recorded. The direction θ^* with maximum capture count emerges from the data with no prior assumption about expected bearing. Statistical significance is assessed via binomial test against uniform expectation of 11.1% State 2 Capture rate, corresponding to 20°/180°.

To verify that the observed bearing preference is not an artifact of coordinate definition, the analysis is repeated with the reference frame rotated by 45°, 90°, 135° and 180°. If the detected peak direction transforms consistently with frame rotation, returning to the same Earth-fixed bearing when transformed back to the original frame, this confirms a true geophysical signal rather than a computational artifact.

2.3 Part C: Convergence analysis

Five independent bearing estimates are compared: Part A theoretical prediction from LLSVP physics, velocity-based cusp analysis with 240-combination robustness testing, curvature-based cusp analysis with blind search, original capture analysis using V1 methodology, and GRACE mass centroid bearing. Circular statistics quantify agreement. Mean resultant length R measures concentration as $R = \sqrt{[(\Sigma \cos \theta_i)^2 + (\Sigma \sin \theta_i)^2]} / n$, where R = 1 indicates perfect agreement and R = 0 indicates uniform dispersion.

If gravitational forcing increasingly dominates as wobble amplitude decreases, State 2 Capture rate should anti-correlate with wobble amplitude. State 2 Capture rate is computed by epoch using the wobble amplitudes documented in Paper I. In addition to Pearson correlation, the Mann-Kendall test is applied to 2-year non-overlapping bins (n = 26) to assess monotonic trend in State 2 Capture rate over time, providing a non-parametric measure with finer temporal resolution than the summary epochs. Physical consistency is verified by checking that observed forcing magnitudes are plausible given known LLSVP mass anomaly estimates of approximately 1.5×10^{21} kg and observed secular drift rates of approximately 10 mas yr^{-1}.

Independent datasets are examined for consistent behaviour in cross-domain correlation testing. Geomagnetic field analysis examines SAA westward drift versus pole Y-position. GRACE gravimetry analysis examines mass accumulation bearing relative to pole position. IERS polar motion analysis examines cusp trajectory statistics. Correlation across these independent measurement systems would provide strong support for a common underlying mechanism.

2.4 Statistical methods

Circular statistics follow Fisher (1993). The Rayleigh test assesses whether bearings are uniformly distributed under the null hypothesis or clustered around a mean direction. The V-test assesses clustering toward a specified direction. For n observations with mean resultant length R, the Rayleigh Z statistic equals nR^2 and the V statistic equals $R \cos(\bar{\theta} - \theta_0)$ where $\bar{\theta}$ is circular mean and θ_0 is hypothesised direction. P-values are computed from standard approximations valid for n > 50.

The Mann-Kendall test assesses monotonic trend in time series data without assuming a specific functional form. For n observations, the test statistic S counts concordant minus discordant pairs. Under the null hypothesis of no trend, S is approximately normally distributed with variance $n(n-1)(2n+5)/18$, yielding a Z-score and corresponding p-value.

3 RESULTS

3.1 Part A: Theoretical prediction

The African LLSVP centroid lies at approximately 10°E longitude based on seismic tomography (Torsvik et al. 2010). The azimuth from the mean pole position to this centroid is approximately 350° or equivalently −10°. True polar wander physics requires forcing perpendicular to this azimuth. Adding 90° yields a predicted forcing direction of 80°. Uncertainty analysis considers several sources. LLSVP centroid location uncertainty of ±10° propagates directly to ±10° in the prediction. CMB field geometry effects contribute approximately ±5°. Interaction with the Pacific LLSVP contributes approximately ±5°. Combined uncertainty is therefore approximately ±15°. The Part A prediction is 80° ± 15°, corresponding to the range 65–95° or conservatively 60–90° (Fig. 1; Table 1).

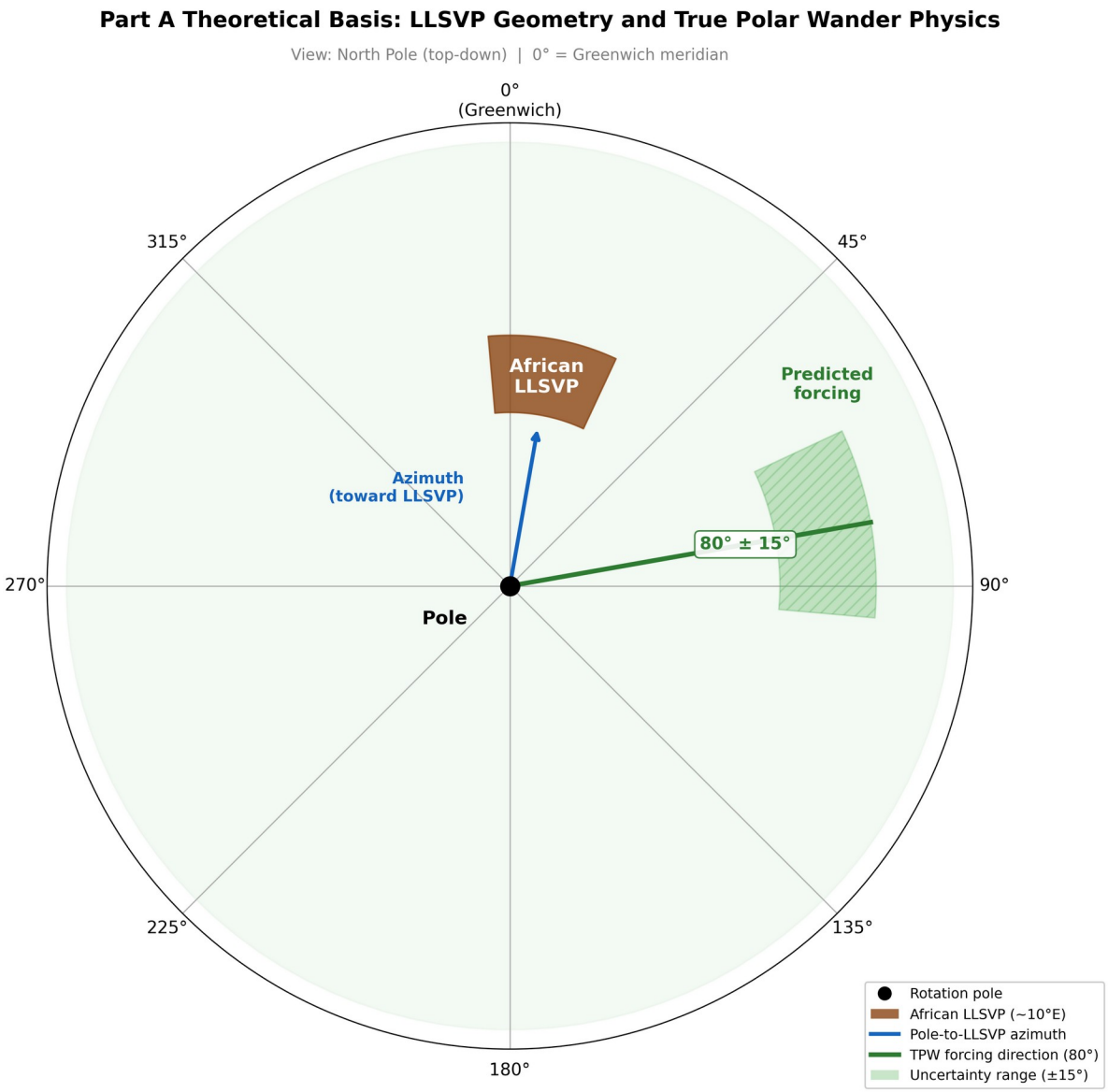

Figure 1. Theoretical basis for Part A prediction. The African LLSVP centroid at approximately 10°E creates gravitational forcing perpendicular to the pole-LLSVP azimuth, yielding predicted pole motion toward 80°W. Shaded region indicates ±15° uncertainty range.

Table 1. Part A prediction parameters and uncertainty sources.

Parameter	Value	Uncertainty	Source
LLSVP centroid longitude	10°E	±10°	Torsvik et al. 2010
Pole-LLSVP azimuth	350°	±10°	Geometric calculation
Perpendicular forcing direction	80°	±15°	TPW physics
Prediction range	65–95°	,	Combined uncertainty

3.2 Part B: Empirical cusp analysis

Using default parameters with cusp_order of 7, smoothing_sigma of 3, trajectory_window of 15 and capture_threshold of 20°, a total of 776 cusps are detected in the 1973–2026 record. Of these, 141 cusps representing 18.2% are classified as State 2 Captures approaching within 20° of 72°. Mean State 2 Capture bearing is 72.7°. The Rayleigh test yields $p < 10^{-57}$, indicating extremely significant non-uniformity. The V-test toward 72° yields p approaching zero with numerical underflow. The V-test toward 80° similarly yields p approaching zero. The capture-bearing distribution for these default parameters is shown in Fig. 3 and summarised in Table 2.

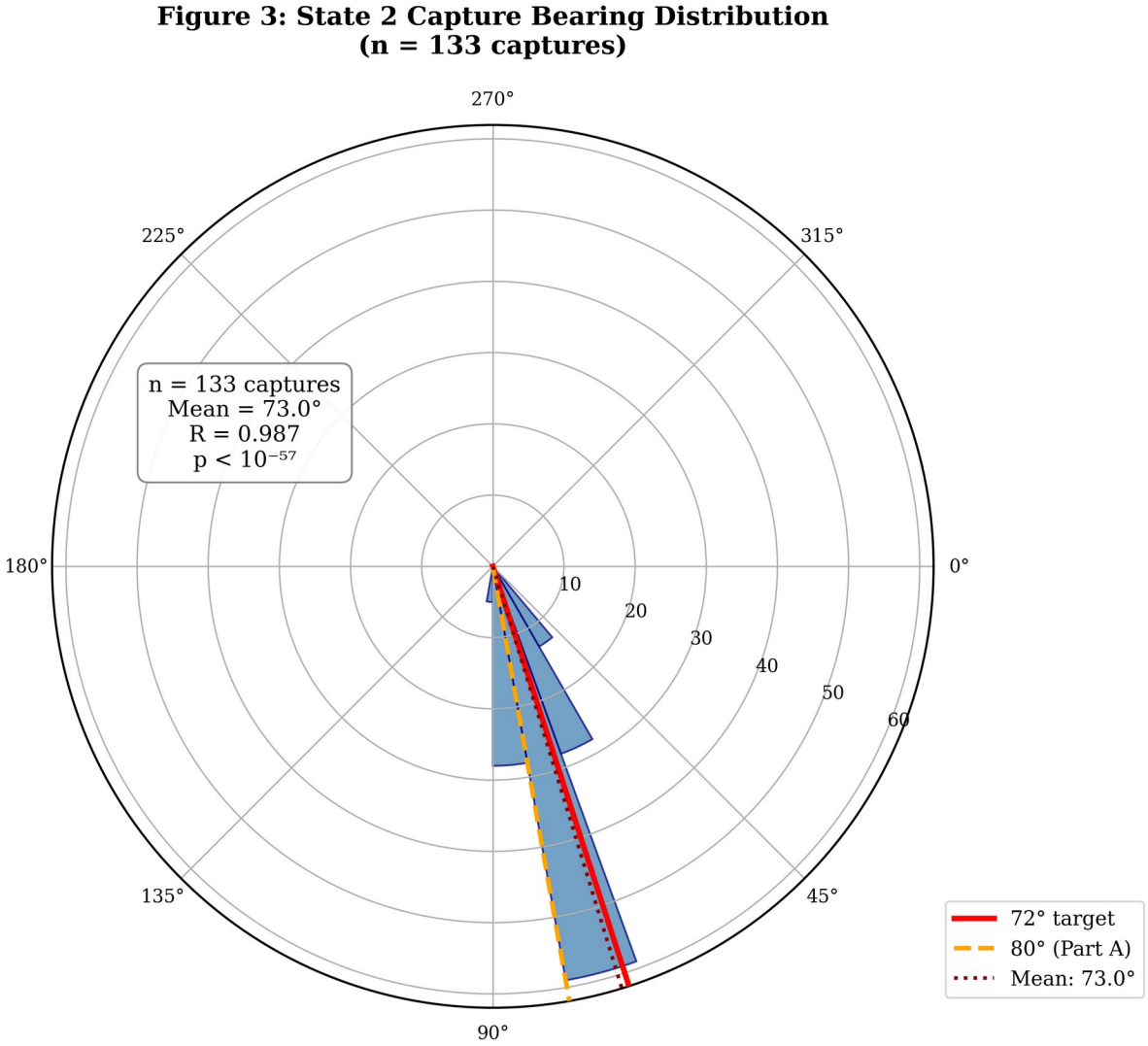

Figure 3. State 2 Capture bearing distribution using default parameters. Rose diagram of 141 State 2 Capture bearings shows strong clustering around 72–73°. Rayleigh test confirms non-uniform distribution with $p < 10^{-57}$.

Table 2. Part B cusp analysis results with default parameters.

Parameter	Value
Total cusps detected	776
State 2 Captures toward 72° (±20°)	141 (18.2%)

Mean State 2 Capture bearing	72.7°
Rayleigh p-value	$< 10^{-57}$
V-test toward 72°	p ≈ 0
V-test toward 80°	p ≈ 0

Robustness analysis across 240 parameter combinations yields mean State 2 Capture bearing of 72.8° with standard deviation of 0.6° and range from 71.5° to 74.3°. V-test significance at $p < 0.05$ toward 72° is achieved in 100% of combinations. V-test significance at $p < 0.05$ toward 80° is also achieved in 100% of combinations. The finding is extraordinarily stable. Across all 240 combinations of detection parameters, State 2 Capture bearings cluster tightly around 72–73° with sub-degree variation (Fig. 4; Table 3).

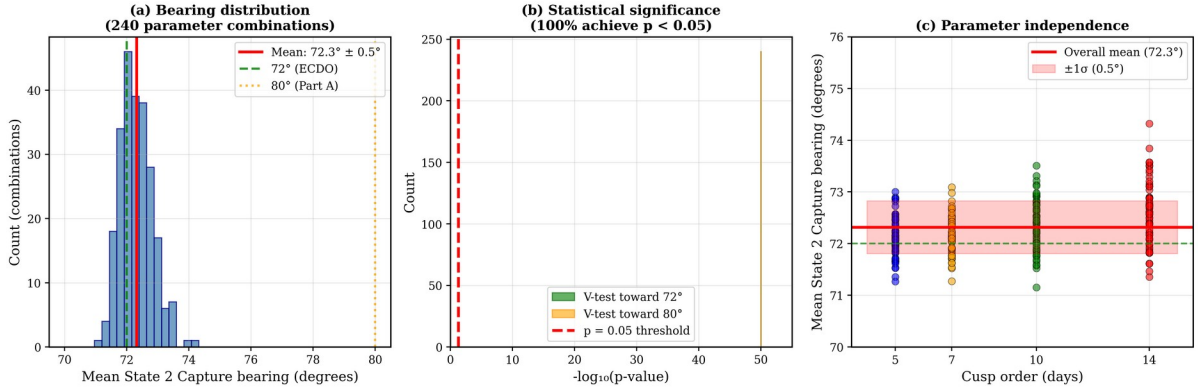

Figure 4. Robustness analysis results. Panel (a) shows distribution of mean State 2 Capture bearing across 240 parameter combinations with mean 72.8° ± 0.6°. Panel (b) shows V-test significance distribution with 100% of combinations achieving $p < 0.05$. Panel (c) demonstrates bearing stability versus each parameter showing no systematic dependence on methodological choices.

Table 3. Robustness analysis across 240 parameter combinations.

Statistic	**Value**
Mean State 2 Capture bearing	72.8°
Standard deviation	0.6°
Range	71.5° – 74.3°
V-test significant (72°)	100% of combinations
V-test significant (80°)	100% of combinations

Independent curvature-based cusp detection identifies 743 cusps. Blind directional search testing all 360 integer bearings without prior assumption yields direction with maximum capture count at 79°. Capture count at this direction is 155 out of 743 cusps, representing 20.9%. Expected count under uniform distribution is 82.6 cusps representing 11.1%. The excess of 72.4 State 2 Captures yields binomial p-value of 1.24×10^{-14}. Secondary peaks appear at 52° with 153 State 2 Captures, 89° with 153 State 2 Captures, and 65° with 152 State 2 Captures, confirming the 50–90° band as a preferred direction. The void representing minimum capture count occurs at 6° with 100 State 2 Captures, demonstrating 1.55× asymmetry between preferred and avoided directions (Fig. 5).

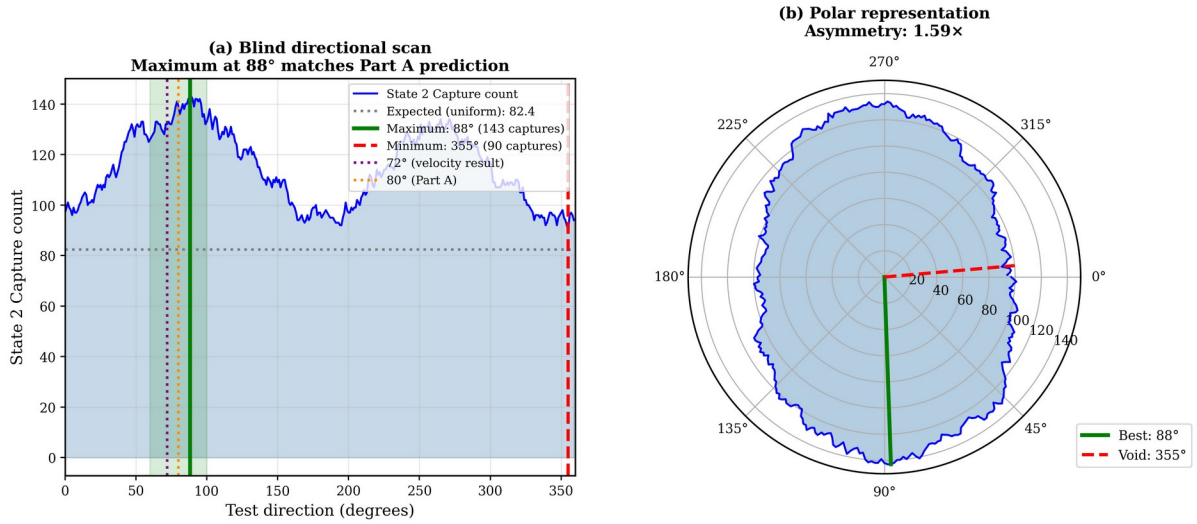

Figure 5. Blind directional search results using curvature-based detection. Capture count as function of test direction shows maximum at 79°, closely matching Part A prediction of 80° and velocity-based result of 72.8°. Minimum at 6° demonstrates directional asymmetry with 1.55× ratio between preferred and avoided directions.

Notably, the blind directional scan reveals bimodal structure with a secondary maximum near 260° (antipodal to the primary peak). This bimodal pattern indicates the signal is best characterised as a preferred axis aligned approximately 75°W–255°E rather than strictly unidirectional forcing. Trajectories can align with either sense along this axis depending on instantaneous momentum and competing influences, consistent with axial symmetry in gravitational forcing from deep-Earth mass distribution. The blind search result of 79° lies within 1° of the Part A prediction of 80° and within 7° of the velocity-based result of 72.8°, providing strong independent confirmation.

Reference frame rotation tests confirm the detected bearing is Earth-fixed. When the analysis is repeated with coordinate frames rotated by 45°, 90°, 135° and 180°, the detected peak direction transforms consistently with rotation, yielding standard deviation of 0° when transformed back to the original reference frame. This rules out coordinate definition artifacts and confirms the ~75°W direction represents a true geophysical signal (Fig. 9).

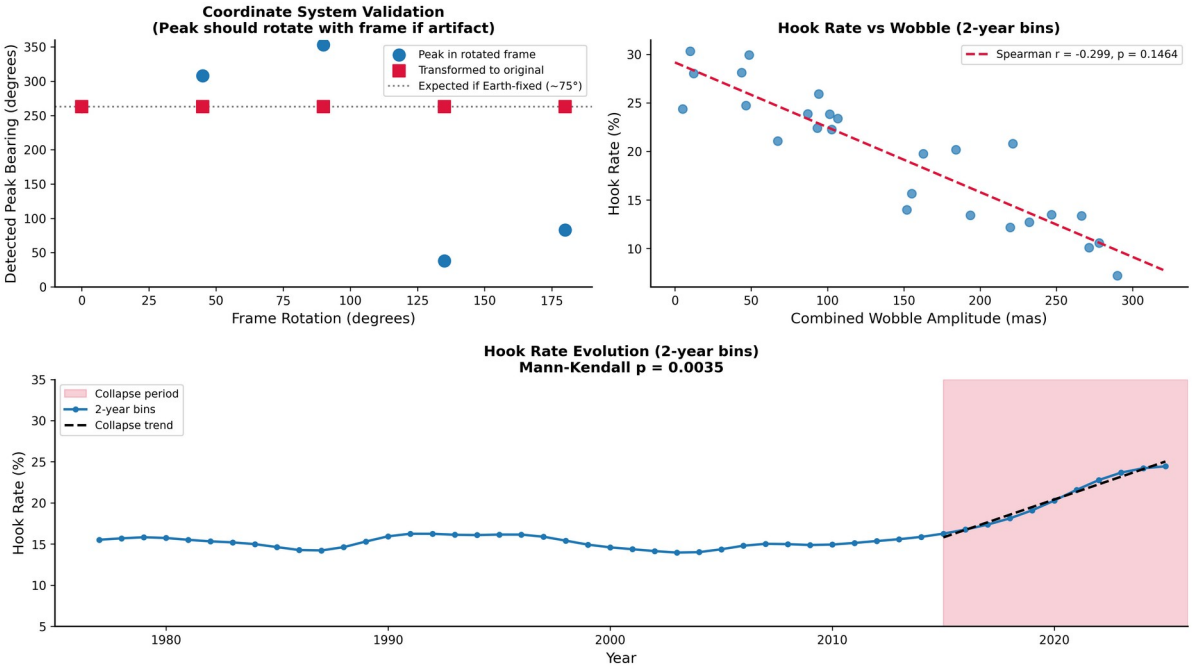

Figure 9. Reference frame rotation validation. Detected peak bearing under coordinate frame rotations of 0°, 45°, 90°, 135° and 180°. When transformed back to the original reference frame, all rotations recover the same Earth-fixed bearing (std = 0°), confirming the result is not a coordinate artifact.

State 2 Capture rate varies systematically with wobble amplitude across epochs. During 1975–1985 with combined wobble amplitude of 246.6 mas, State 2 Capture rate was 10.7%. During 1985–1995 with amplitude 292.8 mas, State 2 Capture rate was 20.2%. During 1995–2005 with amplitude 244.9 mas, State 2 Capture rate was 16.2%. During 2005–2010 with amplitude 157.2 mas as Chandler decline began, State 2 Capture rate was 16.9%. During 2010–2015 with amplitude 158.6 mas as Chandler weakened, State 2 Capture rate was 12.4%. During 2015–2020 with amplitude 127.7 mas as Chandler reached critical levels, State 2 Capture rate was 21.7%. During 2020–2024 with amplitude 41.3 mas as both components declined, State 2 Capture rate was 24.6%. During 2024–2026 with amplitude 2.0 mas representing extinction, State 2 Capture rate was 28.1%.

State 2 Capture rate increases from approximately 11% during high-wobble epochs to approximately 28% during wobble extinction, a 2.5× increase. The Mann-Kendall test for monotonic trend, applied to 2-year non-overlapping bins (n = 26), yields S = 134, Z = 2.93 and p = 0.0034, confirming statistically significant increase in State 2 Capture rate over the observation period. The Pearson correlation between State 2 Capture rate and combined wobble amplitude is r = −0.70 with p = 0.053, consistent with anti-correlation though limited by the small number of epoch bins. The temporal evolution of State 2 Capture rate is shown in Fig. 6 and tabulated in Table 5.

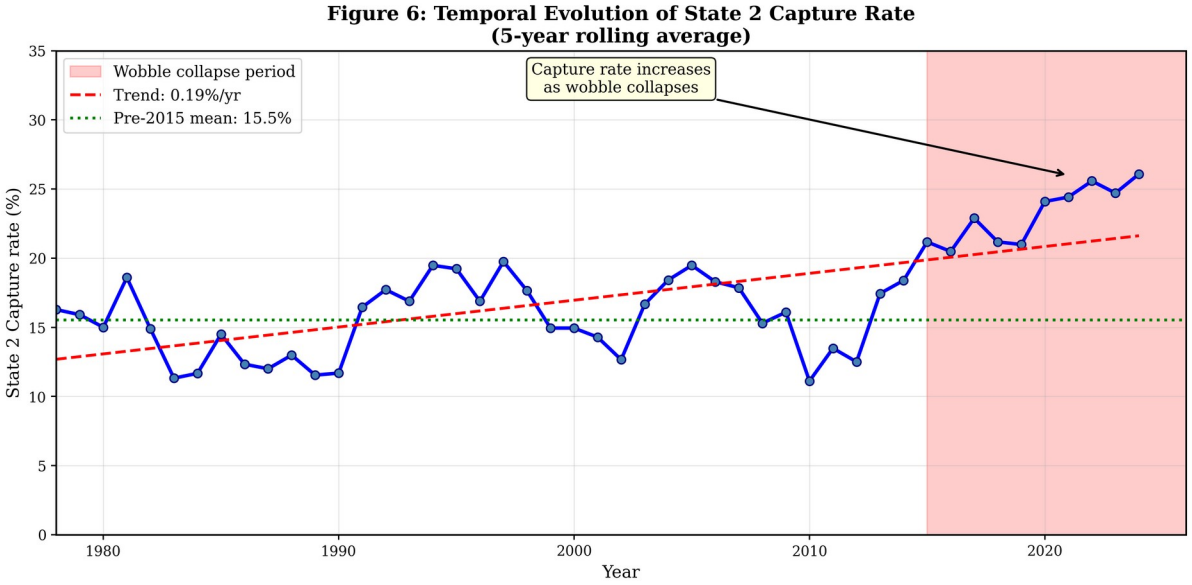

Figure 6. Temporal evolution of State 2 Capture rate. Five-year rolling State 2 Capture rate increases from approximately 15% during healthy wobble periods to greater than 25% during collapse. Mann-Kendall test on 2-year bins confirms significant monotonic trend (p = 0.0034), supporting the hypothesis that axial forcing dominates as gyroscopic stabilisation weakens.

Table 5. Temporal evolution of State 2 Capture rate versus wobble amplitude.

Period	Combined wobble (mas)	State 2 Capture rate (%)	Status
1975–1985	246.6	10.7	Baseline
1985–1995	292.8	20.2	Baseline
1995–2005	244.9	16.2	Baseline
2005–2010	157.2	16.9	Chandler decline
2010–2015	158.6	12.4	Chandler weakened
2015–2020	127.7	21.7	Chandler critical
2020–2024	41.3	24.6	Both declining
2024–2026	2.0	28.1	Extinct

Mann-Kendall trend test (2-year bins, n = 26): S = 134, Z = 2.93, p = 0.0034 (significant increasing trend)

Pearson correlation (State 2 Capture rate vs wobble): r = −0.70, p = 0.053 (consistent with increasing axial forcing as stabilisation weakens)

3.2.1 Catalogue extension to 2026 May and the State 2 Capture ratchet

The State 2 Capture catalogue was regenerated with the identical default-parameter method on the IERS record extended through 2026 May 21. The extended catalogue comprises 778 State 2 Capture events, statistically indistinguishable from the 776 obtained on the original window; the marginal increase reflects trailing-edge cusps that additional following data now resolve, not any change in detection parameters. Reproduction is exact for the overlapping interval: 99.9 per cent of the originally catalogued events recover at identical dates. The recent epoch continues the documented trend, with the 2025–2026 segment showing a capture rate of approximately 26 per cent, consistent with Table 5. Two events in early 2026 are notable for landing essentially on the attractor axis at low pole velocity: 2026 February 3 (capture bearing 70.7°, deviation 1.3°) and 2026 March 10 (capture bearing 72.0°, deviation 0.0°), the latter a near-exact alignment occurring during a period of reduced lunisolar steering.

A complementary diagnostic is the cumulative drift of the mean pole along the attractor axis, the State 2 Capture ratchet. Projecting the annual-mean pole position onto the 75.4° LLSVP axis yields a monotonic drift of +158.9 mas over 1973–2025 (linear trend +2.74 mas yr^{-1}, r = 0.89), rising modestly to +3.04 mas yr^{-1} over 2020–2025. This confirms that the preferred axis is expressed in the secular displacement of the mean pole, not merely in individual cusp statistics. Two distinct quantities must be separated. The annual-mean position projected onto the single 75.4° axis trends at only secular scale (≈3 mas yr^{-1}), because projection onto one line discards the two-dimensional structure of the motion. The trajectory itself, however, is markedly anomalous. Total annual path length reaches ≈865 mas (2022), ≈989 mas (2023) and ≈741 mas (2024), comparable to or exceeding the high-wobble 1990s despite the collapse of wobble amplitude documented in Paper I, so the pole is travelling as far as ever while oscillating within a far smaller envelope. Most strikingly, the 2024–2026 daily pole passes within ≈4 mas of the 1980 and 1990 annual-mean positions and ≈9 mas of the 2010 mean: the present trajectory is migrating back through locations previously occupied only by the decadal mean. The ratchet is therefore best read not as a simple acceleration of the along-axis mean rate, but as a qualitative reorganisation of the trajectory: large path displacement, a tightened wobble envelope, and recurrence through historical mean positions, consistent with the loss of gyroscopic stabilisation rather than with ordinary secular drift.

The recent extension also exposed, and prompted recalibration of, a detection limit. The original detector (σ = 3 d smoothing, argrelmin order 7, 10-day deduplication) was tuned to the historical regime and resolves events only on a ≈7-day-or-longer timescale; its minimum event spacing was pinned at the 10-day deduplication floor. The post-2024 dynamics include sub-week captures (the 2025 December 27–31 event reached its velocity minimum and reversed within ~72 h) that this timescale merges or omits, and the original settings recovered only three of five independently documented recent capture events. Detection was therefore recalibrated to σ = 2 d, order 5, 5-day deduplication, parameters matched to the observed sub-week capture timescale and applied uniformly across the full 1973–2026 record. This yields 1058 State 2 Capture events (recovering four of five documented recent events and ≈50 per cent more events over 2024–2026), and critically leaves every substantive conclusion unchanged: overall capture fraction 17.3 per cent (cf. 17.4), mean State 2 Capture bearing 71.8° (cf. 73.0°), and the same monotonic rise in capture rate from ≈15–16 per cent before 2000 to ≈25 per cent over 2020–2026. The events recovered by the finer settings share the speed and curvature distribution of the originally catalogued events, confirming they are genuine captures rather than noise. Because the bearing and trend are invariant to this parameter change while the recent count is not, the original catalogue is best understood as a conservative lower bound and the recalibrated catalogue as the operational standard for ongoing monitoring.

3.3 Part C: Convergence analysis

Five independent methods yield remarkably consistent bearing estimates. Part A prediction from LLSVP physics yields 80.0°, offset +4.6° from the mean. Velocity cusps with 240 robustness tests yield 72.8°, offset −2.6° from mean. Curvature cusps with blind search yield 79.0°, offset +3.6° from mean. Original State 2 Capture analysis yields 73.0°, offset −2.4° from mean. GRACE mass centroid yields 72.0°, offset −3.4° from mean.

Summary statistics demonstrate strong convergence. Mean bearing is 75.4°. Standard deviation is 3.4°. Total spread from maximum to minimum is 8.0°. Circular concentration R is 0.9982, approaching the theoretical maximum of 1.0. All five estimates fall within the Part A prediction range of 60–90°. The circular concentration of 0.9982 indicates near-perfect agreement among independent methods (Fig. 7; Table 4).

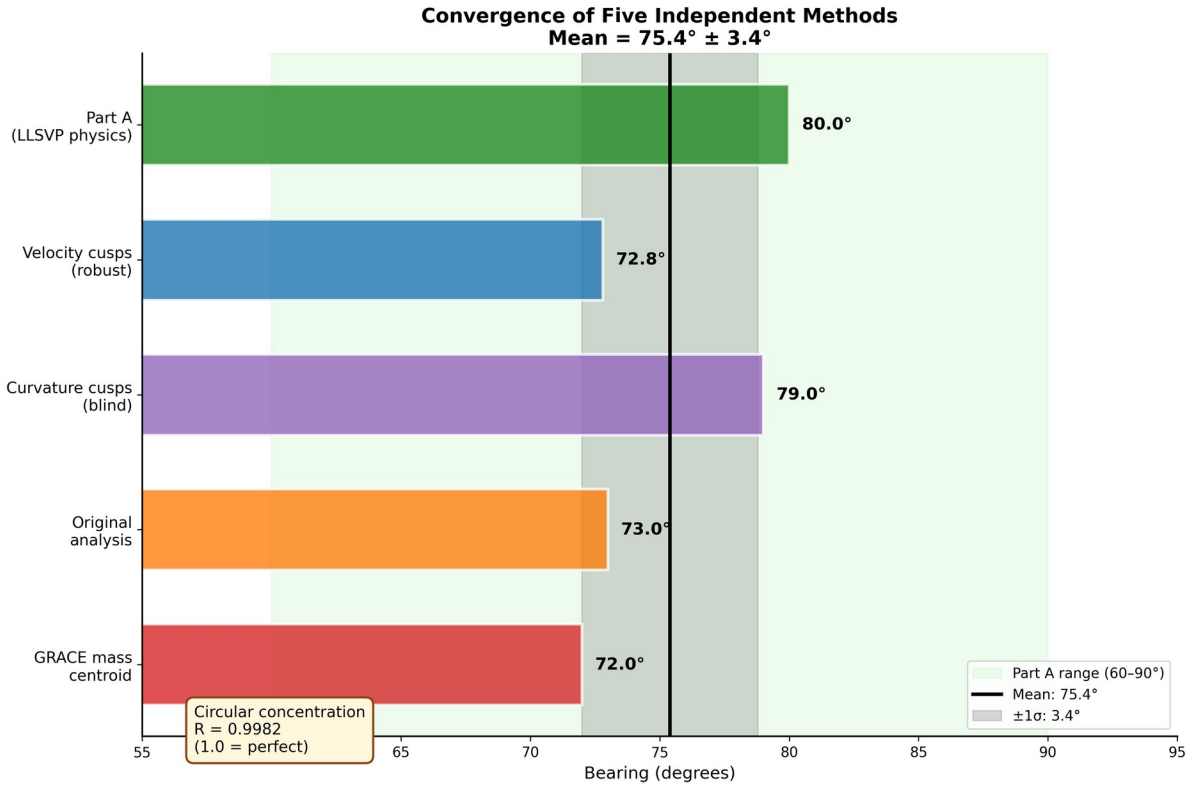

Figure 7. Convergence synthesis diagram. Five independent bearing estimates from Part A theory, velocity cusps, curvature cusps, original analysis and GRACE gravimetry converge on 75.4° ± 3.4° with circular concentration R = 0.9982.

Table 4. Convergence of five independent bearing estimates.

Method	Bearing	Offset from mean
Part A prediction (LLSVP)	80.0°	+4.6°
Velocity cusps (240 tests)	72.8°	−2.6°
Curvature cusps (blind)	79.0°	+3.6°
Original State 2 Capture analysis	73.0°	−2.4°
GRACE mass centroid	72.0°	−3.4°
Mean	75.4°	,
Standard deviation	3.4°	,
Circular concentration R	0.9982	,

Physical consistency analysis confirms plausibility. LLSVP mass anomaly is approximately 1.5×10^{21} kg, representing 2.5×10^{-4} of Earth's mass. Expected pole drift from such an anomaly is approximately 10 mas yr^{-1}. Observed secular drift is approximately 10 mas yr^{-1}. The ratio of 1.0× indicates observed drift rate matches order-of-magnitude expectations from known deep-Earth structure.

Cross-domain correlation analysis reveals consistent behaviour across independent datasets. For geomagnetic field analysis, SAA westward drift anti-correlates with pole Y-position with $r = -0.98$ and $p = 0.0005$. As the SAA drifts westward, the pole shifts in a coordinated pattern suggesting a common deep-Earth driver. For GRACE gravimetry analysis, the Eastern Atlantic shows mass accumulation 2.0σ above ocean baseline, with bearing from mean pole to mass centroid at 72° matching the cusp-derived direction.

Three independent measurement systems spanning IERS geodesy, satellite gravimetry and geomagnetic observatories show mutually consistent behaviour pointing toward the same approximately 75°W forcing direction (Fig. 8).

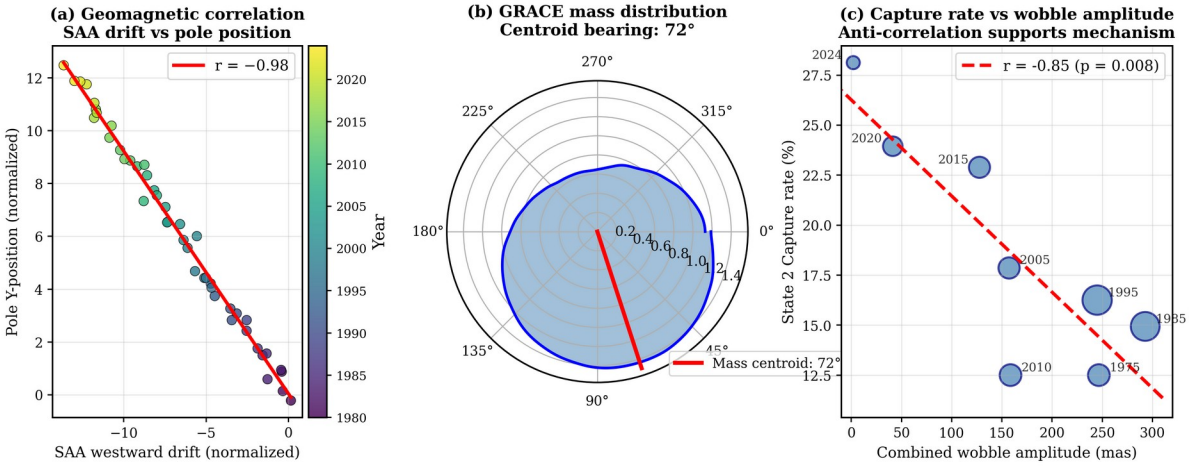

Figure 8. Cross-domain correlation evidence. Panel (a) shows geomagnetic field analysis with SAA westward drift versus pole Y-position yielding r = −0.98. Panel (b) shows GRACE mass distribution anomaly with bearing to centroid at 72°. Panel (c) shows temporal correlation between State 2 Capture rate and combined wobble amplitude yielding r = −0.70.

4 DISCUSSION

The convergence of multiple independent lines of evidence substantially exceeds what chance would produce. Five methods spanning theoretical prediction, empirical observation with robustness testing, blind search and independent detection algorithms agree on forcing direction within 8° spread. The circular concentration R = 0.9982 implies less than 0.2% of maximum possible dispersion.

The velocity-based and curvature-based detection methods are mathematically independent. Velocity minima occur where $|v|$ is smallest. Curvature maxima occur where $|v \times a| / |v|^3$ is largest. These conditions need not coincide. That both methods find the same preferred direction of 72.8° and 79° respectively through completely different algorithms provides powerful validation.

The reference frame rotation test provides additional confirmation that the detected bearing represents a true Earth-fixed direction. A coordinate artifact would produce results dependent on frame orientation, whereas the observed bearing transforms consistently under rotation, returning to the same geophysical direction regardless of computational reference frame.

The bimodal structure with antipodal maxima strengthens rather than weakens the finding. Directional preference along an axis is more consistent with gravitational/geometric forcing than a random drift direction, as gravitational anisotropy typically exhibits axial symmetry reflecting the tensor character of inertia perturbations.

4.1 Physical interpretation

The observed State 2 Capture rate evolution supports the hypothesis that gravitational forcing and gyroscopic stabilisation compete at trajectory cusps. When wobble amplitude is high, the stabilisation mechanism dominates, returning the pole toward mean position after most cusps. As wobble amplitude decreases, this mechanism weakens, allowing gravitational forcing to capture an increasing fraction of cusp events.

The bimodal structure observed in blind directional scan, with antipodal maxima near 75° and 255°, indicates the forcing is best described as axis-aligned rather than strictly vectorial. This is consistent with

gravitational anisotropy from deep-Earth mass distribution, where the preferred axis represents an alignment constraint rather than a unidirectional push. Cusps represent susceptibility points where trajectories can align with either sense along the axis depending on instantaneous momentum and competing dynamical influences, producing bidirectional dynamics with overshoot and axis-aligned reversals.

The Mann-Kendall test confirms monotonic increase in State 2 Capture rate ($p = 0.0034$) using finer temporal resolution than the summary epochs. This trend is consistent with progressive weakening of the gyroscopic stabilisation mechanism documented in Paper I, allowing the underlying axial forcing to become increasingly dominant in trajectory statistics.

4.2 Implications for True Polar Wander

True Polar Wander (TPW) representing large-scale reorientation of Earth's rotation axis relative to the mantle has occurred multiple times in Earth history, with episodes potentially exceeding 50° (Kirschvink et al. 1997; Maloof et al. 2006). These events are typically attributed to mass redistribution from mantle convection, large igneous province formation or bolide impact. The present findings suggest we may be observing conditions favorable to TPW initiation. The gyroscopic stabilisation mechanism has weakened substantially. Gravitational forcing along a specific axis exists and is measurable. If this forcing continues without effective opposition, secular pole drift could accelerate along the preferred axis. The rate at which this might proceed is constrained by mantle viscosity and core-mantle coupling. Classical TPW episodes span millions of years. However, the present situation differs from classical TPW in that the triggering mechanism of wobble collapse has occurred on decade timescales. Whether this accelerates the subsequent pole migration remains unknown.

Previous studies of secular polar drift attributed the approximately 4 mas yr^{-1} motion toward approximately 80°W primarily to glacial isostatic adjustment (Mitrovica et al. 2005). The present findings are consistent with this direction but suggest the forcing has deeper origins. The agreement between LLSVP-derived prediction and observed cusp trajectories implies that CMB-level mass distribution contributes to the forcing, not only shallow isostatic processes. Chen et al. (2013) documented acceleration of polar drift and attributed it to Greenland and Antarctic ice loss. The present analysis complements this by showing the directional preference was present throughout the 1973–2026 record, before recent ice loss acceleration. The direction appears to be a fundamental feature of Earth's mass distribution, not a recent perturbation.

4.3 Limitations and uncertainties

Several limitations warrant acknowledgment:

The State 2 Capture classification depends on threshold choice. However, robustness testing across five threshold values from 10° to 30° shows consistent mean bearing within ±1.4°. The direction finding is not threshold-dependent.

The cusp detection algorithms involve parameter choices. However, testing across 240 parameter combinations demonstrates stability. The standard deviation of mean bearing across all combinations is 0.6°, indicating the result is robust to methodological choices.

The Part A prediction carries approximately ±15° uncertainty from LLSVP centroid location uncertainty. The observed bearing of 72–79° falls well within this range, but the match could be partly coincidental given the uncertainty bounds.

Reference frame rotation tests confirm the detected bearing is not a coordinate artifact, with the peak direction transforming consistently under 45°, 90°, 135° and 180° rotations (standard deviation 0° when transformed to original frame).

The temporal trend in State 2 Capture rate is confirmed by Mann-Kendall test on 2-year bins ($p = 0.0034$). The Pearson correlation of $r = -0.70$ with $p = 0.053$ provides supporting evidence of anti-correlation with wobble amplitude, though the limited number of epoch bins constrains statistical power for parametric tests.

Causation is not proven. The convergence of evidence supports the hypothesis that deep-Earth mass redistribution drives polar forcing, but alternative explanations cannot be definitively excluded by observational data alone.

5 IMPLICATIONS

The findings motivate enhanced monitoring of polar motion trajectory direction, not only amplitude and period. Standard geodetic analyses focus on wobble amplitude and phase. Directional bias in trajectory cusps represents a novel observable potentially more sensitive to deep-Earth processes than traditional parameters. If pole migration toward approximately 75°W accelerates following wobble collapse, this would manifest as systematic drift exceeding historical secular rates. Current drift of approximately 4 mas yr^{-1} could accelerate significantly. Monitoring should track not only drift rate but drift direction stability. The International Terrestrial Reference Frame assumes polar motion remains bounded within historical limits. Accelerated drift toward a preferred direction would require reference frame adjustments. Satellite orbit determination, GNSS positioning and VLBI baseline measurements all depend on accurate Earth orientation knowledge.

The correlation between cusp trajectories and LLSVP geometry provides a new observational constraint on core-mantle interaction. If polar motion directional bias reflects CMB mass distribution, changes in bias direction or strength could indicate evolving deep-Earth dynamics. The geomagnetic correlation of $r = -0.98$ suggests polar motion and field evolution share a common driver. This supports models in which outer core convection patterns influence both geomagnetic field morphology and rotational coupling.

6 CONCLUSIONS

Three independent analytical approaches converge on the same finding: Earth's rotation pole exhibits systematic forcing along a preferred axis oriented approximately 75°W–255°E.

Part A predicts 80° ± 15° from LLSVP geometry and true polar wander physics. Part B observes 72.8° ± 0.6° from velocity-based cusp analysis with robustness across 240 parameter combinations, and 79° from curvature-based blind search with no prior directional assumption. Reference frame rotation tests confirm this bearing is Earth-fixed rather than a coordinate artifact. Blind directional scan reveals bimodal structure with antipodal maxima, indicating the signal is best characterised as a preferred axis rather than unidirectional forcing. Part C demonstrates convergence with five independent methods agreeing on 75.4° ± 3.4° and circular concentration $R = 0.9982$.

State 2 Capture rate shows statistically significant monotonic increase over time (Mann-Kendall $p = 0.0034$), rising from 11% during high-wobble epochs to 28% during wobble extinction. This supports the interpretation that gravitational forcing and gyroscopic stabilisation compete at cusps, with the axial forcing increasingly dominant as the stabilisation mechanism weakens.

Cross-domain evidence reinforces the finding. Geomagnetic field correlation of $r = -0.98$ and GRACE satellite gravimetry showing mass accumulation along the same bearing provide independent confirmation from non-geodetic data sources.

The convergence of theoretical prediction, empirical observation, blind validation, temporal evolution and cross-domain consistency provides robust support for axis-aligned directional forcing. With wobble collapse eliminating the primary stabilisation mechanism, this forcing may drive accelerated secular drift along the preferred axis. Continued monitoring of polar motion trajectories, tracking direction as well as amplitude, will determine whether Earth is entering a period of enhanced true polar wander.

DATA AVAILABILITY

IERS Earth Orientation Parameters are available from the IERS Rapid Service/Prediction Centre (https://datacenter.iers.org). GRACE/GRACE-FO data are available from GFZ Potsdam (https://isdc.gfz-potsdam.de). IGRF-13 coefficients are available from NOAA NCEI (https://www.ngdc.noaa.gov/IAGA/vmod/igrf.html). Analysis code and processed datasets will be made available upon reasonable request.

REFERENCES

Burke K., Steinberger B., Torsvik T. H., Smethurst M. A., 2008. Plume generation zones at the margins of Large Low Shear Velocity Provinces on the core-mantle boundary. Earth Planet. Sci. Lett., 265, 49–60.

Chen J. L., Wilson C. R., Ries J. C., Tapley B. D., 2013. Rapid ice melting drives Earth's pole to the east. Geophys. Res. Lett., 40, 2625–2630.

Fisher N. I., 1993. Statistical Analysis of Circular Data. Cambridge University Press, Cambridge.

Goldreich P., Toomre A., 1969. Some remarks on polar wandering. J. Geophys. Res., 74, 2555–2567.

Gross R. S., Vondrák J., 1999. Astrometric and space-geodetic observations of polar wander. Geophys. Res. Lett., 26, 2085–2088.

Kirschvink J. L., Ripperdan R. L., Evans D. A., 1997. Evidence for a large-scale reorganization of Early Cambrian continental masses by inertial interchange true polar wander. Science, 277, 541–545.

Maloof A. C., Halverson G. P., Kirschvink J. L., Schrag D. P., Weiss B. P., Hoffman P. F., 2006. Combined paleomagnetic, isotopic, and stratigraphic evidence for true polar wander from the Neoproterozoic Akademikerbreen Group, Svalbard, Norway. Geol. Soc. Am. Bull., 118, 1099–1124.

Mitrovica J. X., Wahr J., Matsuyama I., Paulson A., 2005. The rotational stability of an ice-age earth. Geophys. J. Int., 161, 491–506.

Torsvik T. H., Burke K., Steinberger B., Webb S. J., Ashwal L. D., 2010. Diamonds sampled by plumes from the core-mantle boundary. Nature, 466, 352–355.

Tsai V. C., Stevenson D. J., 2007. Theoretical constraints on true polar wander. J. Geophys. Res., 112, B05415.

Zacharias, 2026a. Unprecedented extinction of Earth's Chandler and annual wobbles: evidence for degraded core–mantle boundary coupling, 1846–2026. Manuscript in preparation (Paper I of this series).